IEEE Access
Multidisciplinary | Rapid Review | Open Access Journal

Received 2 July 2023, accepted 1 August 2023, date of publication 7 August 2023, date of current version 15 August 2023.

Digital Object Identifier 10.1109/ACCESS.2023.3303329

RESEARCH ARTICLE

A Safety Monitoring Method for Anchor Cable Prestress During Slope Construction Based on Spatial Clustering and a Bayesian Panel Vector Autoregression Model

LIN CHENG, YUE JIANG, CHUNHUI MA, JIE YANG, JIAMIN CHEN, SHUAI YUAN, AND ZENGGUANG XU

State Key Laboratory of Eco-Hydraulics in Northwest Arid Region, Xi'an University of Technology, Xi'an 710048, China
Institute of Water Resources and Hydro-Electric Engineering, Xi'an University of Technology, Xi'an 710048, China

Corresponding author: Chunhui Ma (shanximachunhui@foxmail.com)

This work was supported in part by the National Natural Science Foundation of China under Grant 51409205, in part by the State Key Program of National Natural Science of China under Grant 52039008, in part by the Natural Science Basic Research Project of Shaanxi Province under Grant 2023-JC-YB-358, and in part by the Key Scientific Research Project of Shaanxi Provincial Department of Education (Coordination Centre Project) under Grant 22JY044.

ABSTRACT During the construction of water conservancy and hydropower projects, the time series of safety monitoring data for slope engineering is often short. When establishing a slope safety monitoring model, it is necessary to study the modelling method under small sample conditions and closely examine the space–time information in the monitoring data for the limited length of each measuring point. To this end, this paper initially proposes using the Ward clustering method to spatially cluster anchor cable prestress measuring points in different parts of a slope; then, according to the clustering results, a safety monitoring model for slope anchor cable prestress is established for each type of measuring point based on a Bayesian panel vector autoregressive (BPVAR) model with highly accurate small sample modelling. Finally, slope anchor cable prestress monitoring data in China are taken as examples for verification analysis. The analysis results show that the prestressed measuring points of the slope anchor cable for this project are divided into four categories: excavation causes the prestress of some slope measuring points to continue to increase, and the tension or compression of the structural plane leads to an increase or decrease in prestress. The multiple correlation coefficients of the training set and test set data of the BPVAR model are all above 0.80, and the prediction error of the validation set is less than that of the vector autoregressive (VAR) model, the autoregressive moving average (ARMA) model and the long short-term memory (LSTM) model. The measured prestress values are all within the 95% confidence interval, which provides a reference for safety state identification in slope engineering.

INDEX TERMS Construction period, slope safety monitoring, ward clustering method, Bayesian panel vector autoregressive (BPVAR) model, prestress of anchor cable.

I. INTRODUCTION

In recent years, with the construction of large-scale water conservancy and hydropower projects, many high and steep slopes with complex safety conditions have been formed after excavation [1]. The safety of high slopes in water conservancy projects is an important issue related to water conservancy and hydropower facilities and public safety and property. The stability of a slope is usually affected by many factors [2], [3], including geological conditions, rainfall, groundwater level fluctuations and seismic loads [4]. Among them, construction excavation and disturbance are important reasons

The associate editor coordinating the review of this manuscript and approving it for publication was Wentao Fan.

for the rapid evolution of the slope safety state during construction [5]. High slopes in water conservancy projects are mostly located in alpine canyons, where rock mass stability is already compromised. Excavation disturbance leads to slope stress redistribution [6], which creates a significant unloading effect. Prestressed anchor cables are an effective reinforcement method to improve the safety of high slopes [7], [8], [9]. An anchor cable is a stress-absorbing structure buried deep underground that can greatly improve the stability of rock and soil structures [10]. However, if the prestress of the anchor cable is reduced to a certain limit, instability or failure can occur [11]. Under the action of a large anchoring load, a rock mass will deform with time, which is the main reason for the loss of prestress. This change in prestress in an anchor cable is related to the strength and structural characteristics of the rock mass [12]. When the rock mass is hard and complete, the prestress loss of the anchor cable is relatively small, while the prestress loss of an anchor cable anchored in a weak fracture rock mass is relatively large [13]. Therefore, monitoring slope anchor cable prestress is important for understanding slope safety status. After obtaining the monitoring data, interpreting the data and quantitatively predicting possible outcomes become the key challenges [14].

The time series of slope safety monitoring data during construction is often short, and there is often a lack of environmental monitoring data. A traditional statistical model with various environmental factors as influencing factors has poor applicability. The time series model provides a set of data processing methods with a scientific basis, which essentially analyses the internal structure and complex characteristics of the data to enable prediction [15], [16]. Many researchers have analysed the time series characteristics of slope data through various techniques [17]. Aggarwal et al. [18] used an autoregressive differential moving average model, generalized autoregressive conditional heteroscedasticity model and dynamic neural network model to predict univariate time series and compared them. Meng et al. [19] used the H-P filtering method to decompose trend and periodic terms from slope time series, used the model to process the trend terms smoothly and calculate the predicted value of the trend terms, and used the vector autoregressive model to calculate the predicted value of the periodic terms, thus improving the prediction effect. Lu et al. [20] decomposed the time series by variational mode decomposition, used a one-dimensional cubic piecewise function to train and predict the trend term, and used a fruit fly optimization algorithm and variational mode decomposition model to train and predict the periodic term and random term. Their results showed that the model can effectively improve prediction accuracy. However, the above time series model only considered the analysis from the time dimension. Xu et al. [21] proposed that an organic combination and comprehensive analysis of the time–space evolution law is an important guarantee for the accurate prediction of slope monitoring data. Zhao et al. [22] used an interdisciplinary method combining small baseline subset interferometric synthetic aperture radar, deep displacement monitoring and engineering geological surveys to identify the deformation mechanism and spatiotemporal characteristics of a slope. Feng et al. [23] obtained the spatial and temporal distribution characteristics of rainfall-induced group landslides through satellite remote sensing images, rainfall monitoring data and artificial rainfall physical models and explained the rainfall instability mechanism of slopes. Based on monitoring data, Cheng et al. [24] established a statistical regression model to analyse the temporal and spatial evolution of slope deformation during the impoundment of a reservoir bank and simulated the slope deformation and failure process under impoundment conditions based on regression analysis. Ge et al. [25] introduced the basic theory of spatial econometrics and the dynamic panel data analysis method, established a dynamic spatial panel data model of slope displacement, and tested the spatial prediction ability of the model. Thus, there is consensus for slope safety monitoring models to combine the time evolution law and spatial distribution characteristics of slope monitoring data.

Compared with a traditional time series model, the panel data model of a time series can fully exploit and utilize the effective information of monitoring data in time and space and has good spatial and temporal prediction effects. The vector autoregressive (PVAR) model based on panel data is an extension of the vector autoregressive (VAR) model from plane to space. This model reduces the requirement of data length in modelling and has good application prospects [26], [27], [28]. The advantage of modelling multiple time series (panel data) at the same time is to obtain more accurate prediction results by collecting data rather than using only a single sequence of data. [29] In general, the least squares method, moment estimation method, and maximum likelihood estimation method are used to estimate the parameters of the PVAR model. Table 1 lists the estimation methods, applicability and characteristics of several classic time series models [30], [31], [32], [33]. Pesaran [34] noted that due to cross-sectional heterogeneity, traditional methods are no longer applicable to panel data. Zellner [35] and Canova and Ciccarelli [36] applied the Bayesian estimation method to the PVAR model. Under the assumption of prior information, the posterior distribution of the model was obtained by the Gibbs sampling method, and the estimated value of the parameters was obtained. This can achieve predictive analysis involving multiple periods in the future [37] and has often shown good performance for time series modelling and analysis in the case of small samples. Compared with several traditional estimation methods of the PVAR model, the Bayesian panel vector autoregressive (BPVAR) model has improved mathematical properties that are suitable for the short-term prediction analysis of panel data, and it has the advantage of fewer model estimation parameters when considering the spatial and temporal information of panel data.

TABLE 1. Comparison of classical time series models.

Model	Method of estimation	Serviceability	Feature
VAR	Least squares	Short-term prediction for multivariate time series	There are more parameters to be estimated, and the operation is simple
ARMA	Moment estimation, least squares, maximum likelihood	Stationary time series prediction	There are few parameters to be estimated, and the operation is complicated
ARIMA	Moment estimation, least squares, maximum likelihood	Nonstationary time series forecasting	The model is simple but cannot capture the nonlinear relationship
PVAR	Generalized moment, least squares, maximum likelihood	Panel data prediction	It offers space-time prediction, but there are many parameters to be estimated.
BPVAR	Bayesian estimation	Short-term forecast of panel data	It offers spatiotemporal prediction and fewer parameters to be estimated.

Because the multipoint monitoring data for a slope anchor cable dynamometer include not only the time series information but also the spatial information [25], the prediction accuracy of the slope anchor cable prestress safety monitoring model can be improved by fully excavating and utilizing the effective information of the short-sequence monitoring data in time and space during the construction period. Therefore, this paper proposes using the Ward clustering method to perform spatial clustering analysis on prestressed monitoring data during the construction of the slope and using the BPVAR model to establish a unified safety monitoring model for each type of measuring point, which addresses the difficulty of modelling the monitoring data of the prestressed short sequence of the slope anchor cable during the construction period. Finally, the application effect of the prestressed safety monitoring model of the slope anchor cable proposed in this paper is verified by a slope engineering example.

II. DESCRIPTION OF THE PROBLEM

A large number of anchor cable dynamometers are usually arranged on the slope to observe whether the prestress of the slope is abnormal, as shown in Fig. 1(a). Because the slope prestress monitoring data contain both the cross-sectional data of multiple measuring points and the time series of a single measuring point, the slope prestress monitoring data can be regarded as typical panel data, as shown in Fig. 1(b). Panel data clustering analysis is a research trend in spatiotemporal data mining. Its main goal is to divide objects in space according to the basic characteristics of sample data so that highly similar objects are placed into the same category. The monitoring data of anchor cable prestress of slope have typical characteristics of spatio-temporal variation. It is expected that better prediction results can be obtained when the spatio-temporal correlation of measuring points is considered in modeling. Therefore, the spatial clustering analysis of prestressed measuring points can fully explore the correlation and spatial variation characteristics of prestress. After the clustering analysis, the prestressed measuring points of the slope are divided into several categories, and the prestressed measuring points in each category have highly similar variation laws of the measured values.

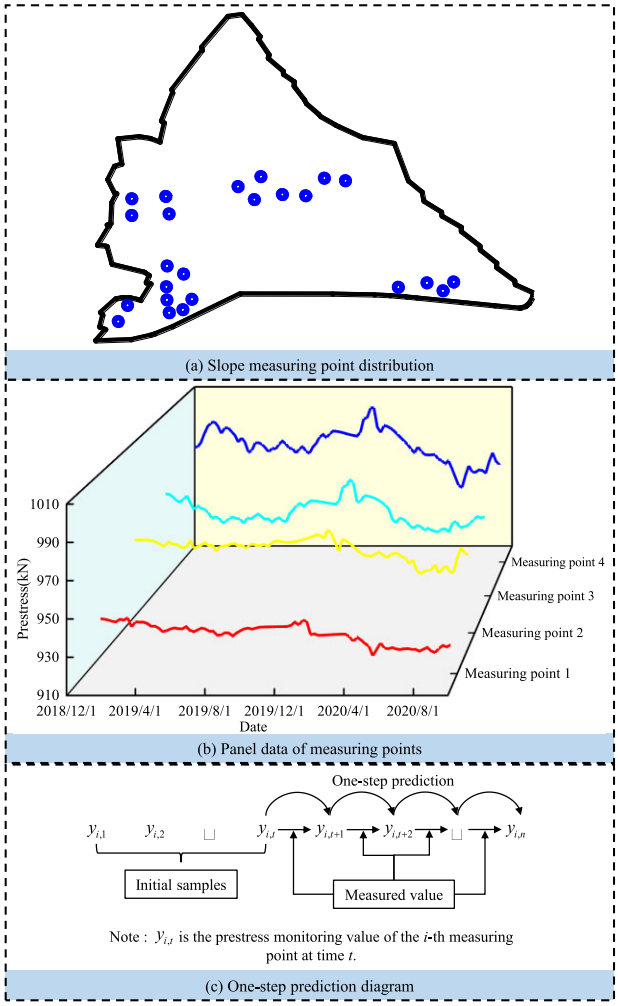

FIGURE 1. One-step prediction diagram of slope panel monitoring data.

Through cluster analysis, different types of prestressed panel monitoring data can be obtained. At this time, a reasonable prediction model should be established to monitor the prestressed safety state of the slope. However, the monitoring data of various environmental quantities in the process of prestress monitoring during slope construction are often not perfect, and it is often difficult to establish traditional

statistical models or machine learning models based on intelligent algorithms. Compared with the traditional modelling method, the time series model can predict the future prestress only through the previously measured values, which can solve key problems such as an imperfect environmental quantity during the construction period. At the same time, the construction period monitoring data are typically small sample data. The Bayesian method has obvious advantages in modelling small sample data and can address the challenge of a small amount of data. Considering that the prestress monitoring data contain a large amount of time and space information, this paper uses the panel data model to predict the prestress and quantitatively analyse the safety state of the prestress through the model prediction results.

In summary, this paper uses the spatial clustering method to conduct in-depth excavation of the prestressed monitoring data during the slope construction period and uses the Bayesian estimation method of the panel data model to predict and analyse the prestressed panel data, as shown in Fig. 1(c). Through the prediction results of the panel data model, researchers can determine whether the prestress of the slope is within the normal range to achieve slope prestress safety monitoring.

III. BASIC THEORIES AND METHODS

A. WARD SPATIAL CLUSTERING ANALYSIS

The application of data mining in the field of safety monitoring has become increasingly widespread [38], [39]. Cluster analysis is a typical data mining method. Common clustering analysis methods include partition clustering and hierarchical clustering. In practical applications, the Ward clustering method is a hierarchical clustering method that offers a relatively good classification effect [40]. Therefore, this paper uses the Ward clustering method for spatial clustering. According to Reference [41], a reasonable clustering method should consider the change value, change rate and change trend of each measuring point.

This paper mainly considers the change characteristics of the measuring point from the following three aspects: 1) the magnitude of the prestress measurement of measuring point i at time t, denoted as x_{it}; 2) the numerical change of measuring point i at time t, denoted as y_{it}; and 3) the magnitude of the value change of measuring point i at time t, denoted as z_{it}. The units and orders of magnitude of the abovementioned three kinds of variation characteristics are inconsistent, and it is obviously unreasonable to directly add the three to obtain the ''comprehensive clustering index''. Therefore, it is necessary to standardize x_{it}, y_{it}, and z_{it} before calculating the comprehensive similarity index. This paper uses the Z score method to normalize the underlying metrics.

Suppose that δ_{it} represents the change index of measurement point i at time t and uses d_{ij} to represent the degree of similarity between measurement point i and measurement point j. Taking the square of Euclidean distance (SED) as the similarity index and taking the prestress measurement values of measuring point i and measuring point j at time t as an example, the SED is

$$d_{ijt}(\mathrm{SED}) = (\delta_{it} - \delta_{jt})^2 \tag{1}$$

where δ_{it} and δ_{jt} represent the prestress measurement values of measuring points i and j at time t, respectively.

Taking measuring point e and measuring point f as an example, this paper defines three basic similarity indicators: 1) the absolute distance of the measuring point, denoted as $d_{ef}^{S}(AD)$; 2) the incremental distance of the measuring point, denoted as $d_{ef}^{S}(KD)$; and 3) the speed-up distance of the measuring point, denoted as $d_{ef}^{S}(GRD)$. The above three similarity indicators are shown in Formulas (2)–(4):

$$d_{ef}^{S}(\mathrm{AD}) = \sum_{t=1}^{T} (x_{et} - x_{ft})^2 \tag{2}$$

$$d_{ef}^{S}(\mathrm{KD}) = \sum_{t=1}^{T} (y_{et} - y_{ft})^2 \tag{3}$$

$$d_{ef}^{S}(\mathrm{GRD}) = \sum_{t=1}^{T} (z_{et} - z_{ft})^2 \tag{4}$$

In the formulas, $x_{et} = \delta_{et}$, $x_{ft} = \delta_{ft}$, $y_{et} = x_{et} - x_{e,t-1}$, $y_{ft} = x_{ft} - x_{f,t-1}$, $z_{et} = \frac{y_{et}}{x_{e,t-1}}$, and $z_{ft} = \frac{y_{ft}}{x_{f,t-1}}$.

The three basic similarity indices are fused to obtain a comprehensive similarity index, which is used to measure the overall similarity of different measurement points. This paper considers this the comprehensive distance between measuring point e and measuring point f, abbreviated as $d_{ef}^{S}(\mathrm{CD})$, as shown in Formula (5):

$$d_{ef}^{S}(\mathrm{CD}) = d_{ef}^{S}(\mathrm{AD}) + d_{ef}^{S}(\mathrm{KD}) + d_{ef}^{S}(\mathrm{GRD}) \tag{5}$$

For the slope prestress monitoring data, including G periods and M measuring points, the squared deviation sum of the M_u measuring points within the panel data classification H_u can be obtained as:

$$W_{tu} = \sum_{i=1}^{M_u} \left[(x_{itu} - \bar{x}_{tu})^2 + (y_{itu} - \bar{y}_{tu})^2 + (z_{itu} - \bar{z}_{tu})^2 \right] \tag{6}$$

If it is divided into j classes, then the global total sum of squared deviations is

$$W = \sum_{t=1}^{G} \sum_{u=1}^{j} W_{tu} \tag{7}$$

where W_{tu} represents the deviation sum of squares of the measured points in period t in H_u; x_{itu}, y_{itu}, and z_{itu} correspond to the three parameters in Formulas (2)–(4); and $\bar{x}_{tu}$, $\bar{y}_{tu}$, and $\bar{z}_{tu}$ represent the parameter average value of M_u measuring points at time t in H_u.

The determination of the number of clusters needs to comprehensively consider the pedigree clustering dendrogram and the change rule of measuring points. In practice, the final number of clusters can be determined by the change in the

inconsistency coefficient in the clustering process, as shown in Formula (8):

$$\xi_i = \frac{l_{i1} - l_{i2}}{l_{i3}} \tag{8}$$

where ξ_i is the inconsistency coefficient of the i-th clustering; l_{i1} is the clustering distance during the i-th clustering; l_{i2} is the mean of the clustering distances during the i-th clustering; l_{i3} is the standard deviation of the clustering distance during the i-th clustering; and i=1, 2, $\cdots$, n-1, where n is the number of samples.

B. BPVAR MODEL THEORY

1) PANEL DATA UNIT ROOT TEST

To test whether the panel monitoring data of slope prestress contain unit roots, this paper considers the following panel autoregressive model [42]:

$$y_{i,t} = \rho_i y_{i,t-1} + z'_{i,t}\gamma_i + \varepsilon_{i,t} \tag{9}$$

In the formula, $i = 1, 2, \cdots, n$ is the cross-sectional unit, $t = 1, 2, \cdots, T_i$ is the time, $z'_{i,t}\gamma_i$ is the individual fixed effect, and $\varepsilon_{i,t}$ is the stationary disturbance term.

Since the disturbance term in Formula (9) may have autocorrelation, Levin et al. [43] proposed the Levin–Lin–Chu (LLC) test method, which introduces a high-order differential lag term to perform the unit root test of panel data:

$$y_{i,t} = \delta y_{i,t-1} + z'_{i,t}\gamma_i + \sum_{j=1}^{p_i} \theta_{ij} y_{i,t-j} + \varepsilon_{i,t} \tag{10}$$

where δ is the common autoregressive coefficient and p_i is the lag order. By introducing a sufficiently high-order differential lag term, the disturbance term $\varepsilon_{i,t}$ can be guaranteed to be white noise.

The limitation of the LLC test is that it requires that the autoregressive coefficients δ of each individual are equal, which may be too zealous in practice. To overcome this shortcoming, Im et al. [44] proposed the Im–Persaran–Shin (IPS) unit root test method for panel data:

$$y_{i,t} = \delta_i y_{i,t-1} + z'_{i,t}\gamma_i + \varepsilon_{i,t} \tag{11}$$

In the formula, δ_i is the regression coefficient of measuring point i, and $\varepsilon_{i,t}$ obeys a normal distribution independent of each other.

A Fisher type test is developed from the augmented Dickey–Fuller (ADF) test. The basic idea of the ADF-Fisher test is similar to the IPS test, where each individual is tested separately and then the information is combined [45]. Specifically, the unit root test is performed on each individual in the panel data to obtain n test statistics and corresponding P values. Choi [46] proposed four methods to synthesize these P values into ''Fisher type'' statistics. In this paper, we use the ''inverse chi-squared transformation'' in four methods:

$$P \equiv -2\sum_{i=1}^{n} \ln p_i \xrightarrow{d} \chi^2(2n), (T_i \to \infty) \tag{12}$$

In the formula: T_i is the time dimension of the measuring point i. Since the negative sign is taken, this is a one-sided right test, that is, the larger the statistic P, the more inclination there is to reject the null hypothesis of ''panel unit root''.

2) THE LAG ORDER TEST OF PANEL DATA

Selecting the order of the panel data is a very important step. Selecting an excessively high lag order will lead to overestimating parameters and model overfitting problems. A low lag order will miss the linear relationship between the monitoring sequence and its lag terms. Therefore, scholars have proposed information criteria to avoid overfitting problems by adding penalty terms for model complexity. The Akaike information criterion (AIC), Bayesian information criterion (BIC) and Hannan–Quinn information criterion (HQIC) are typically used to test the optimal lag order of panel data.

The AIC is a standard used to measure the goodness of model fitting [47]. It is a weighting function of fitting accuracy and the number of unknown parameters. The expression is as follows:

$$AIC = 2k - 2\ln(L) \tag{13}$$

In the formula, k is the number of unknown parameters in the model, and L is the likelihood function in the model.

The BIC is similar to the AIC. Both the AIC and the BIC introduce a penalty term related to the number of model parameters. The penalty term of the BIC is larger than that of the AIC. Considering the number of samples, when the number of samples is too large, it can effectively prevent the model from being too complex due to the high accuracy of the model. The expression of the BIC is as follows [48]:

$$BIC = k\ln(n) - 2\ln(L) \tag{14}$$

In the formula, n is the number of samples.

The HQIC is an improved method of the AIC. The HQIC is also an evaluation criterion based on information entropy, which is typically used to evaluate the fitting degree of different models to data and select the optimal model. The expression of the HQIC is as follows [49]:

$$HQIC = -2\ln(L) + \ln(\ln(n)) \times k \tag{15}$$

3) BAYESIAN ESTIMATION OF THE PANEL VECTOR AUTOREGRESSIVE MODEL

The panel vector autoregressive model includes N measurement points, and each measurement point includes n endogenous variables, p lag terms and T periods. Its general form is as follows:

$$y_{i,t} = \sum_{j=1}^{N}\sum_{k=1}^{p} A_{ij,t}^{k} y_{j,t-k} + C_{i,t}x_t + \varepsilon_{i,t} \tag{16}$$

where $y_{i,t}$ is a $n\times1$ vector of n endogenous variables of measurement point i at time t; $A_{ij,t}^{k}$ is a $n \times n$ coefficient matrix, which represents the response of measurement point i to the kth lag term of measurement point j at time t; x_t is a $m\times1$ vector of exogenous variables; $C_{i,t}$ is a $n\times m$ matrix that associates endogenous variables with exogenous variables;

and $\varepsilon_{i,t}$ is the $n\times 1$ residual vector of measurement point i. In this research, the panel data of the prestressed measuring point should be used as the input model of the endogenous variable, so the exogenous variable x_t is not considered.

This is the general form of a panel vector autoregressive model. In practice, this general form may be too complex to yield accurate estimates. An alternative was proposed by Zellner and Hong [51] that relies on a hierarchical prior recognition scheme, which basically follows the approach of Jarocinski [50]. In the simple method proposed by Zellner and Hong [51], the only parameter estimated is $\boldsymbol{\beta}$, and the vector set is $\boldsymbol{\beta}_i$. Other basic parameters, such as the set of residual covariance matrices $\sum_i$ and the common mean and covariance of the vector autoregressive coefficients $\boldsymbol{b}$ and $\sum_b$, are assumed to be known. The complete posterior distribution of the model can be given by:

$$\pi(\boldsymbol{\beta}, \boldsymbol{b}, \boldsymbol{\Sigma}_b, \boldsymbol{\Sigma}\,|\boldsymbol{y}) \propto \pi(\boldsymbol{y}|\boldsymbol{\beta}, \boldsymbol{\Sigma})\pi(\boldsymbol{\beta}|\boldsymbol{b}, \boldsymbol{\Sigma}_b)\pi(\boldsymbol{b})\pi(\boldsymbol{\Sigma}_b)\pi(\boldsymbol{\Sigma}) \tag{17}$$

In other words, the full posterior distribution is equal to the product of the data likelihood function $\pi(\boldsymbol{y}|\boldsymbol{\beta}, \boldsymbol{\Sigma})$ with the conditional prior distribution $\pi(\boldsymbol{\beta}|\boldsymbol{b}, \boldsymbol{\Sigma}_b)$ for $\boldsymbol{\beta}$ and the prior $\pi(\boldsymbol{\Sigma})$ for $\boldsymbol{\Sigma}$, along with the two hyperpriors $\pi(\boldsymbol{b})$ and $\pi(\boldsymbol{\Sigma}_b)$.

The specific form of the likelihood function is as follows:

$$\pi(\boldsymbol{y}|\boldsymbol{\beta}, \boldsymbol{\Sigma}) \propto \prod_{i=1}^{N} |\bar{\boldsymbol{\Sigma}}_i|^{-1/2} \exp\left(-\frac{1}{2}(\boldsymbol{y}_i - \bar{\boldsymbol{X}}_i\boldsymbol{\beta}_i)'(\bar{\boldsymbol{\Sigma}}_i)^{-1}(\boldsymbol{y}_i - \bar{\boldsymbol{X}}_i\boldsymbol{\beta}_i)\right) \tag{18}$$

The vectors of coefficients $\boldsymbol{\beta}_i$ follow a normal distribution, with common mean $\boldsymbol{b}$ and common variance $\boldsymbol{\Sigma}_b$:

$$\boldsymbol{\beta}_i \sim N(\boldsymbol{b}, \boldsymbol{\Sigma}_b) \tag{19}$$

The prior density for $\boldsymbol{\beta}$ is given by:

$$\pi(\boldsymbol{\beta}|\boldsymbol{b}, \boldsymbol{\Sigma}_b) \propto \prod_{i=1}^{N} |\boldsymbol{\Sigma}_b|^{-1/2} \exp\left(-\frac{1}{2}(\boldsymbol{\beta}_i - \boldsymbol{b})'(\boldsymbol{\Sigma}_b)^{-1}(\boldsymbol{\beta}_i - \boldsymbol{b})\right) \tag{20}$$

The prior distribution for $\boldsymbol{\Sigma}_i$ is simply the classic diffuse prior given by:

$$\pi(\boldsymbol{\Sigma}_i) \propto |\boldsymbol{\Sigma}_i|^{-(n+1)/2} \tag{21}$$

The model must rely on the numerical methods provided by the Gibbs sampler. Therefore, it is necessary to obtain the conditional posterior distribution for each parameter. The complete conditional distribution of $\boldsymbol{\beta}_i$ is as follows: any term in the product that does not involve $\boldsymbol{\beta}_i$ can be classified as a proportional constant:

$$\pi(\boldsymbol{\beta}_i|\boldsymbol{\beta}_{-i}, \boldsymbol{y}, \boldsymbol{b}, \boldsymbol{\Sigma}_b, \boldsymbol{\Sigma}) \propto \pi(\boldsymbol{y}|\boldsymbol{\beta}_i, \boldsymbol{\Sigma})\pi(\boldsymbol{\beta}_i|\boldsymbol{b}, \boldsymbol{\Sigma}_b) \tag{22}$$

of which $\boldsymbol{\beta}_{-i}$ is used to indicate all $\boldsymbol{\beta}$ coefficients minus the $\boldsymbol{\beta}_i$ collection. Due to conditional independence, it is possible to draw each $\boldsymbol{\beta}_i$ in turn by sampling from the corresponding conditional posterior.

The conditional posterior distribution of $\mathbf{b}$ is as follows, and any term not involving $\mathbf{b}$ is classified as a proportional constant:

$$\pi(\boldsymbol{b}|\boldsymbol{y}, \boldsymbol{\beta}, \boldsymbol{\Sigma}_b, \boldsymbol{\Sigma}) \propto \exp\left(-\frac{1}{2}(\boldsymbol{b} - \boldsymbol{\beta}_m)'(\boldsymbol{N}^{-1}\boldsymbol{\Sigma}_b)^{-1}(\boldsymbol{b} - \boldsymbol{\beta}_m)\right) \tag{23}$$

in the formula, $\boldsymbol{\beta}_m = \boldsymbol{N}^{-1}\boldsymbol{\Sigma}_{i=1}^{N}\boldsymbol{\beta}_i$ denotes the arithmetic mean over the $\boldsymbol{\beta}_i$ vectors.

The conditional posterior distribution of $\boldsymbol{\Sigma}_b$ is as follows, relegating to the normalizing constant any term not involving $\boldsymbol{\Sigma}_b$:

$$\pi(\boldsymbol{\Sigma}_b|\boldsymbol{y}, \boldsymbol{\beta}, \boldsymbol{b}, \boldsymbol{\Sigma}) \propto \lambda_1^{-\frac{\bar{s}}{2}-1} \exp\left(-\frac{\bar{v}}{2}\frac{1}{\lambda_1}\right) \tag{24}$$

in the formula, $\bar{s} = h + s_0$ and $\bar{v} = v_0 + \sum_{i=1}^{N}\left\{(\boldsymbol{\beta}_i - \boldsymbol{b})'\boldsymbol{\Omega}_b^{-1}(\boldsymbol{\beta}_i - \boldsymbol{b})\right\}$.

Finally, the conditional posterior distribution is obtained for the set of residual covariance matrices $\boldsymbol{\Sigma}_i$ and relegates to the proportionality constant any term not involving $\boldsymbol{\Sigma}_i$:

$$\pi(\boldsymbol{\Sigma}_i|\boldsymbol{\Sigma}_{-i}, \boldsymbol{y}, \boldsymbol{\beta}, \boldsymbol{b}, \boldsymbol{\Sigma}_b) \propto |\boldsymbol{\Sigma}_i|^{-(T+n+1)/2} \exp\left(-\frac{1}{2}tr\left[\boldsymbol{\Sigma}_i^{-1}\tilde{\boldsymbol{S}}_i\right]\right) \tag{25}$$

Among them, $\tilde{\boldsymbol{S}}_i = (\boldsymbol{Y}_i - \boldsymbol{X}_i\boldsymbol{B}_i)'(\boldsymbol{Y}_i - \boldsymbol{X}_i\boldsymbol{B}_i)$. Due to conditional independence, it is possible to draw each $\boldsymbol{\Sigma}_i$ in turn by sampling from the corresponding conditional posterior distribution.

IV. CONSTRUCTION METHOD FOR SLOPE ANCHOR CABLE PRESTRESS SAFETY MONITORING MODEL

The process of the anchor cable prestress monitoring method during slope construction based on the Ward clustering method and BPVAR model is shown in Fig. 2.

The monitoring method of slope anchor cable prestress based on the Ward clustering method and BPVAR model proposed in this paper mainly involves the following steps:

(1) Data preprocessing. First, according to the layout of the slope monitoring system, prestressed measuring points with high reliability are selected, and the obvious abnormal values in the monitoring data are eliminated. Then, the monitoring data are processed into equidistant sequence data once every 7 days by the linear interpolation method for subsequent modelling. Because the units and dimensions of the characteristic prestress quantities x_{it}, y_{it} and z_{it} are inconsistent, the Z score method is used to standardize the three basic characteristic prestress quantities.

(2) Calculate the three basic similarity indices (absolute distance, incremental distance, and increasing distance) of different measuring points according to Formulas (2)–(4), and then calculate the corresponding comprehensive distance index according to Formula (5). Quantitatively analyse the similarity of spatial measurement points.

(3) Calculate the inconsistency coefficient in each clustering process according to Formula (8) and judge the most

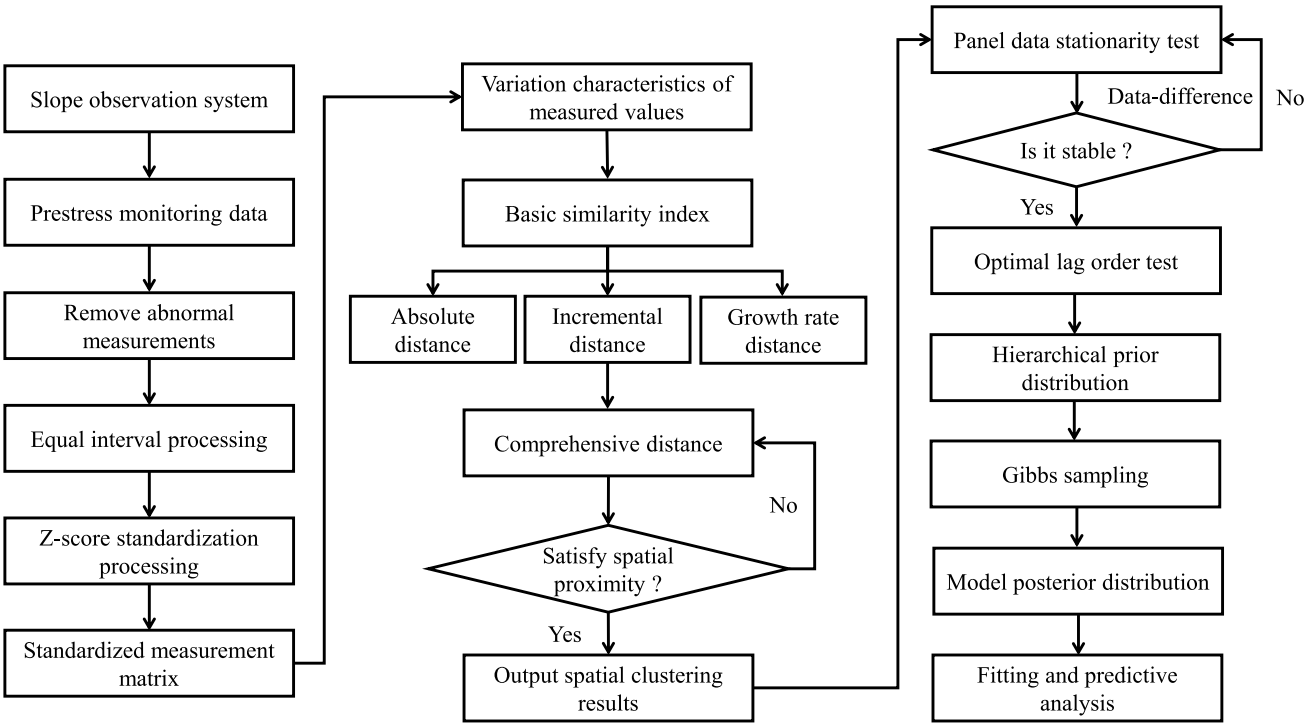

FIGURE 2. The flow chart of the Ward clustering method and BPVAR model.

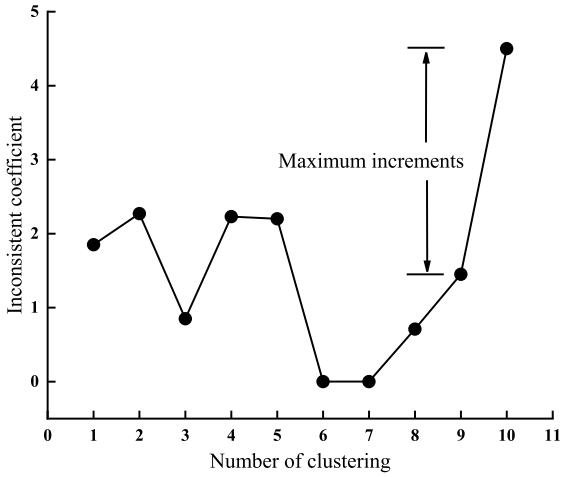

FIGURE 3. Example graph of inconsistent coefficient change in the clustering process.

suitable number of clusters by the increment of the inconsistency coefficient. In the inconsistency coefficient in the Ward clustering process shown in Fig. 3, according to the value of the inconsistency coefficient, it can be seen that the largest increment of the inconsistency coefficient occurs in the penultimate second cluster and the last cluster, and it can be judged that the penultimate second cluster has the best effect.

(4) According to the spatial clustering results of the Ward clustering method, panel data are established for the same type of highly similar measuring points.

(5) According to Formulas (10)–(12), the LLC test, IPS test and ADF-Fisher test are used to test the stability of the panel data of each type of prestressed measuring point.

(6) According to Formulas (13)–(15), the AIC, BIC and HQIC are used to determine the order of the model, and the optimal lag order of the model is determined by the minimum information criterion.

(7) The posterior distribution of the model is derived by the Gibbs sampling method, and the fitting and prediction results are obtained from the posterior probability distribution.

V. PROJECT EXAMPLES

A. PROJECT OVERVIEW

A water conservancy project in China is located in the canyon section of the upper reaches of the Han River. It is located in Yangxian County, east of the Hanzhong Basin in southern Shaanxi Province. It is the first development cascade in the planning for the upper reaches of the Han River. The construction task of the water conservancy project is mainly based on water supply, taking into account power generation and improving water transport conditions. The average annual design water supply of the water conservancy project is 969 million m^3, the normal water level of the reservoir is 450 m, the dead water level is 440 m, the total reservoir capacity of the reservoir is 221 million m^3, and the regulated reservoir capacity is 98 million m^3. The dam adopts a

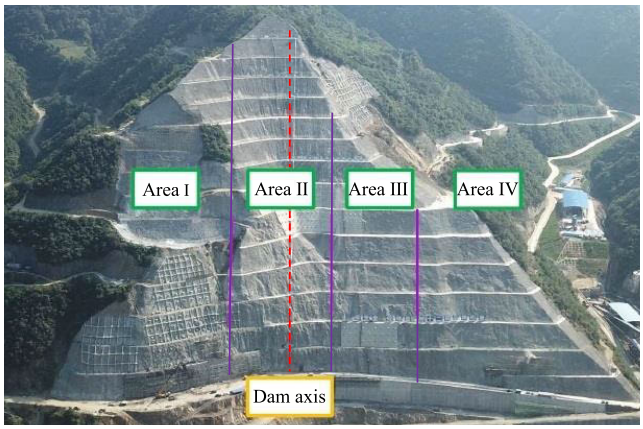

FIGURE 4. Division of left bank slope for a water conservancy project in China.

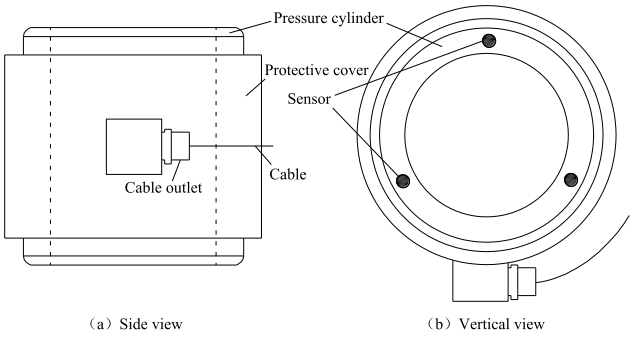

FIGURE 5. Structural diagram of a typical anchor cable dynamometer.

roller-compacted concrete gravity dam with a crest elevation of 455.00 m, a maximum dam height of 63.00 m, and a dam axis length of 349.00 m. The Han River flows into the dam site area from west to east in the northwest of the dam site area, and the flow direction turns to southeast. The river flows 135°, and the river channel is relatively straight. The left bank slope of the dam abutment is 300 m high and more than 400 m long, which represents a very steep and high slope. The slope stratum is an ancient intrusive rock mass with a single lithology, and the main structural types are faults and fissures. The type of groundwater is mainly bedrock fissure water. The depth of the water level is 19.2–35.3 m, and the water level is relatively stable. Under normal conditions, the water level varies from 0.1 to 0.5 m. The slope trend is approximately 315°, the inclination is approximately 225°, the top elevation is 695 m, and the terrain slope is 37∼39°. The slope is set with 3 m wide horse tracks every 15 m high, and the excavation slope ratio is 1:0.3∼1:1.2. Fig. 4 shows a schematic diagram of the left bank slope zoning of the water conservancy project. Fig. 4 shows that the left bank slope is divided into zones I∼IV, of which zone I is the inlet slope of the pump station, and zones II∼IV are the left bank retaining dam section, the powerhouse slope and the power station tailwater slope, respectively.

The construction of the left bank slope of the water conservancy project began in November 2015 and has been completed. The excavation progress and some key events during the slope construction period are shown in Table 2.

B. MONITORING PRINCIPLE AND INSTRUMENT ARRANGEMENT OF ANCHOR CABLE DYNAMOMETER

An anchor cable dynamometer is typically used for slopes to observe the formation and change in prestress, and the temperature can be monitored simultaneously [52]. The installation of the anchor cable dynamometer is shown in Fig. 5. The working principle of the anchor cable dynamometer is as follows: The anchor cable dynamometer is piled on the anchor cable, and the axial pressure borne by the pressure steel pipe of the anchor cable dynamometer will be consistent with the axial tension borne by the anchor cable. When the pressure-bearing steel cylinder is subjected to pressure to produce axial deformation, the strain sensors arranged around the steel cylinder are also deformed synchronously with the steel cylinder. By measuring these strain sensors, the load force borne by the steel cylinder can be calculated so that the axial load borne by the anchor cable can be obtained.

A total of 24 anchor cable dynamometers are arranged on the slope of the water conservancy hub. Nine anchor cable dynamometers, numbered D08ZPR∼D13ZPR and D15ZPR∼D17ZPR, were arranged on the slope of left bank Area I. Three anchor cable dynamometers, numbered D05ZPR∼D07ZPR, were arranged near the 553 m outlet tunnel. After November 2019, due to a change in slope design, anchor cable dynamometers D30ZPR∼D36ZPR and D38ZPR were added. The slope engineering area is located near the Qinling Mountains in China. Affected by multistage tectonic activities and dike intrusion, the structure of the dam area is developed, and the main structural types are faults and fissures. The structural planes revealed in the process of slope excavation are mainly grade IV∼V structural planes, and a small number of grade III structural planes are developed. Among them, there are 14 faults in the slope of Area I and 80 faults in the slope of Areas II∼IV. The larger faults are fz39, F1, F2, f8, fz15 and so on. The monitoring layout and structural plane distribution of the slope anchor cable dynamometer are shown in Fig. 6.

C. SPATIAL CLUSTER ANALYSIS

Because the variation characteristics of slope anchor cable prestress have two dimensions of time and space, and the number of clusters cannot be determined in advance. Therefore, it is more appropriate to use Ward clustering method for spatial clustering analysis in this case. Among the above anchor cable dynamometers, the monitoring sequences of D02ZPR∼D10ZPR, D12ZPR, and D15ZPR∼D16ZPR last more than 1 year, and the measurement point data are reliable. Therefore, the Ward clustering method is used to conduct spatial cluster analysis on the above 12 measurement points. The Z score standardization method is used to standard-

TABLE 2. Excavation progress and key events during the slope construction period.

Date	Key event
November 10, 2015	Start construction
April 2018	The slope treatment in the slump area is completed, the slope in area I is restored to construction, and the slopes in areas II-IV are excavated to the dam abutment elevation
End of May 2018	Obvious deformation of the slope in zone I
End of September to end of October 2018	Blasting excavation is carried out on the slope elevation of 470 m ~ 455 m in zone I
End of December 2018	The deep support of the slope elevation above 470 m in Zone I is completed
End of January to end of February 2019	Excavation of the remaining part of the slope elevation 470 m ~ 455 m in zone I
March 1, 2019	The width of the crack at the slope elevation of 471 m in the area I increases significantly, and the rock mass is broken
Late May 2019	Fault shotcrete cracks appear at zone IV slope elevation 470 m ~ 455 m along the fz15
June 2019	Continuous rain in the project area
August 2019	The fault fz15, fz43, fz43-1 and unstable block KT24 are reinforced
Early September 2019	Continuous rain in the project area
October 2019	Continuous rain in the project area

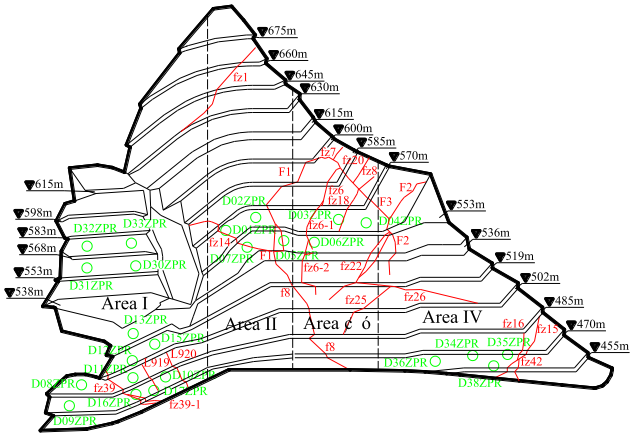

FIGURE 6. Monitoring layout and structural plane distribution of anchor cable dynamometers for slope.

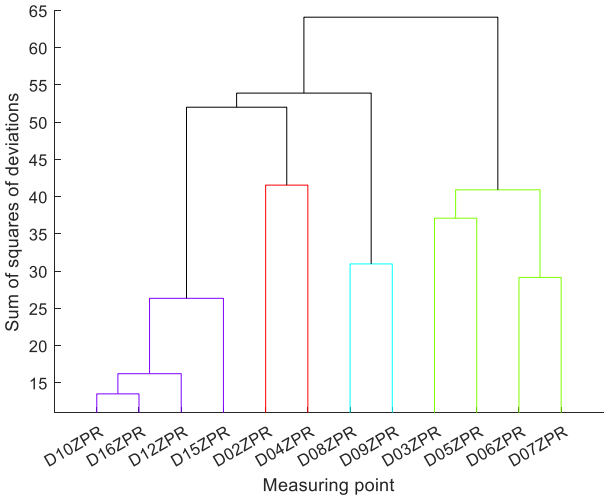

FIGURE 7. Spatial measuring point pedigree clustering tree diagram of the anchor cable dynamometer.

ize the prestress monitoring data of the 12 anchor cable dynamometers. The time section is from December 2018 to September 2020. A total of 91 data points from each anchor cable dynamometer are used in the clustering analysis. The standardized data fluctuation is approximately 0, with a mean of 0 and a standard deviation of 1. After the standardization operation, the value range of the data is further restricted, which avoids the influence of the value range. The prestress monitoring data of the above 12 anchor cable dynamometers were clustered and analysed by the Ward clustering method, and the clustering pedigree dendrogram was obtained as shown in Fig. 7.

The inconsistency coefficient can be used to determine the final number of classifications. In the clustering process, if the inconsistency coefficient corresponding to a certain clustering increases significantly compared with the last incident, it means that the effect of this clustering is poor [53]. The inconsistency coefficients of the above clustering process are obtained by calculation, and the results are 0, 0.7071, 0.7071, 0, 0, 0, 0.8652, 0, 0.9332, 0.6501, and 0.9576. Considering the change in the inconsistency coefficient between the third reciprocal cluster and the fourth reciprocal cluster, the inconsistency coefficient increases significantly by 0.9332, indicating that the effect of the fourth reciprocal cluster is relatively good, so it is most appropriate to divide the prestressed measuring points into four categories. According to the variation in the inconsistency coefficient and the clustering dendrogram, the prestress of the slope anchor cable is divided into four similar regions, as shown in Fig. 8.

To compare with the traditional clustering method, this paper chooses the classic K-means algorithm to cluster the above 12 prestressed measuring points. The basic concept of the K-means clustering algorithm is to select K data as the initial clustering centre, where K is the number of clusters specified by the researchers [54]. The distance from the data point to each initial clustering centre is calculated, and the data points are assigned to the set of each initial clustering centre to form a cluster. The centre of each cluster is updated according to each point in the cluster. The allocation is repeated and the steps are updated until the cluster no longer changes. K-means clustering includes the following steps: (1) Randomly generate the initial cluster centroid.

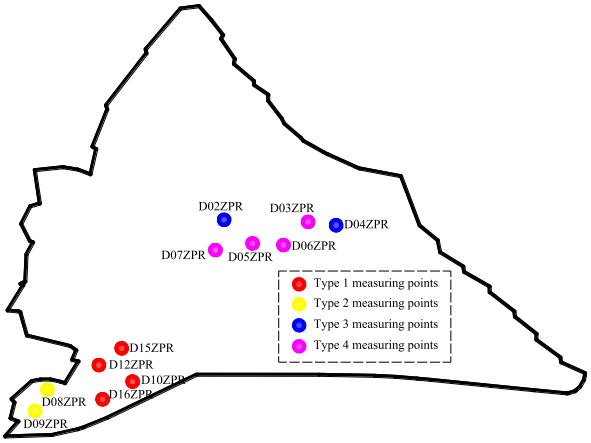

FIGURE 8. Ward clustering results of slope prestress measuring points.

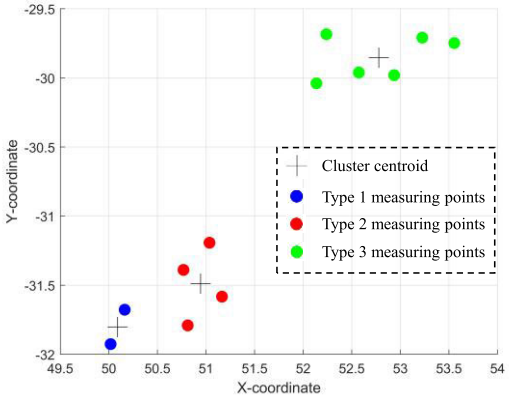

FIGURE 9. K-means clustering results of slope prestress measuring points.

(2) Calculate the Euclidean distance from all samples to the cluster centroid. (3) If the sample is closest to a cluster centroid, then the sample is divided into the cluster; if the Euclidean distance of the sample to multiple cluster centroids is equal, it can be divided into any cluster. (4) After grouping all samples according to Euclidean distance, the mean value of each group is calculated and used as the new clustering centroid. (5) Repeat steps (2)–(4). When the new cluster centroid is equal to the original centroid, the iteration stops, and the algorithm ends. According to the calculation results of the K-means clustering algorithm, the prestress of the slope anchor cable is divided into three similar regions, as shown in Fig. 9.

The K-means clustering results show that the slope prestress measuring points are divided into three categories. The first type of measuring points are D08ZPR and D09ZPR, the second type of measuring points are D10ZPR, D12ZPR, D15ZPR and D16ZPR, and the third type of measuring points are D02ZPR ∼ D07ZPR. The above research shows that the spatial clustering results obtained by the Ward method and K-means algorithm are different. By comparing the two clustering results and the variation law of prestress measurement, it can be seen that the Ward clustering results are more

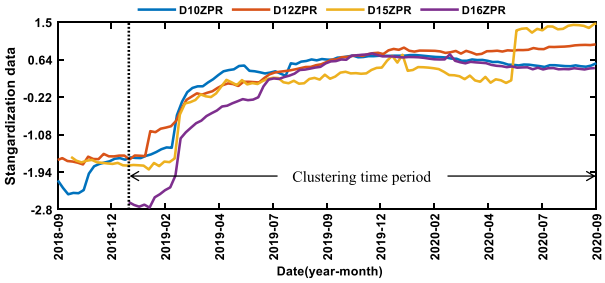

FIGURE 10. The prestressed change curve of the anchor cable of the type 1 measuring points.

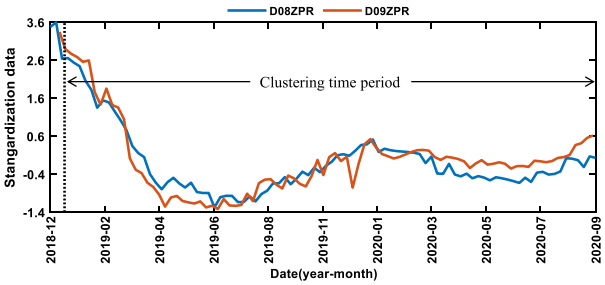

FIGURE 11. The prestressed change curve of the anchor cable of the type 2 measuring points.

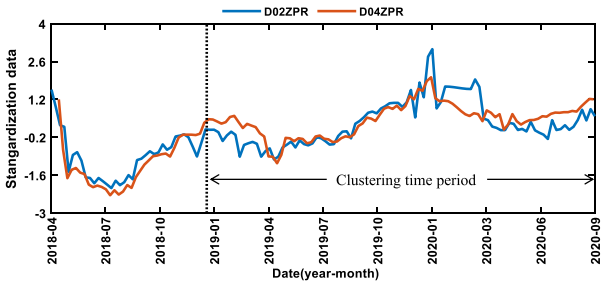

FIGURE 12. The prestressed change curve of the anchor cable of the type 3 measuring points.

consistent with the variation law of anchor cable prestress measurement. Therefore, this paper divides the slope anchor cable prestress into four categories based on the Ward clustering results. The variation law of prestress at each type of measuring point is shown in Fig. 10 ∼ Fig. 13 (the prestress measurements in the figure have been standardized).

Type 1 measuring points are D10ZPR, D12ZPR, D15ZPR and D16ZPR, which are located in the potential block area formed by the structural planes fz39 and L920. As shown in Fig. 10, after the slope anchor cable is locked, the prestress is slightly relaxed due to the combined effects of steel strand retraction and formation compression at the initial stage, and then the prestress continues to increase. After September 2019, it gradually stabilized. The force of the anchor cable continues to change and adjust with the slope deformation. Especially since the slope blasting excavation on February 28, 2019, the growth rate of the force of each anchor cable

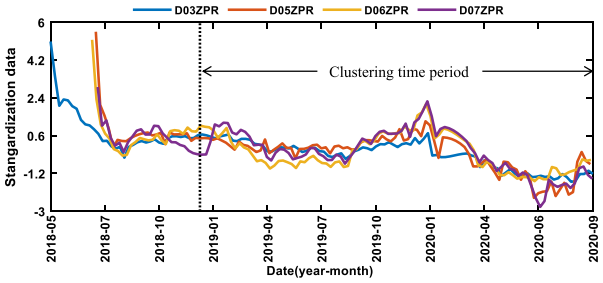

FIGURE 13. The prestressed change curve of the anchor cable of the type 4 measuring points.

has accelerated significantly. D10ZPR, D12ZPR, D15ZPR and D16ZPR are all located in the middle and lower parts of the block, and their measured values show increased growth. The growth time point and change rule are consistent with the nearby multipoint displacement meter, indicating that the stress growth of each anchor cable is mainly caused by the block deformation caused by blasting excavation. The prestress of the first type of measuring points shows an obvious continuous upwards trend, indicating that the slope has an outwards displacement. At the same time, the opening deformation of the structural plane in the slope also leads to the increasing prestress of the anchor cable [55]. From the point of view of the force of the anchor cable, the prestress of the first type of measuring point increases relative to the locking value, and the increment ratio is between 11% and 25%. The measured value of D16ZPR in the lower part of the block increases the most, reaching 24.85% of the locking value, which is also consistent with the larger deformation increment in the lower part of the block.

Type 2 measuring points are D08ZPR and D09ZPR, which are located at the toe of the slope in Area I on the left bank. It can be seen in Fig. 11 that after the self-tensioning and locking of the anchor cable dynamometer, the prestress relaxes rapidly in a short period of time and shows an obvious downwards trend in the early monitoring period. At the same time, the compression deformation of the structural plane in the slope also leads to the rapid relaxation of the anchor cable prestress. At the end of June 2019, heavy rainfall continued in the project area, and rainwater infiltrated and accumulated inside the slope, which increased the sliding of the surface rock mass, which generated an additional anchoring force and weakened the strength of the anchor cable strand [56], causing the prestress to continue to increase. big. By the beginning of 2020, the creep deformation of the rock mass causes rebound shrinkage of the anchor cable, which in turn causes prestress loss of the anchor cable [57] and then gradually stabilizes. As of September 2020, the prestress loss rate was within 5%, the change in the measured value was in line with the general law of anchor cable stress, and the prestress loss range was within the normal range, indicating that the anchor cable stress was basically normal, and the slope was not significantly deformed.

Type 3 measuring points are D02ZPR and D04ZPR, which are located at 570 m elevation of the slope in Areas II∼IV of the left bank. It can be seen in Fig. 12 that after the anchor cable is tensioned and locked, it is affected by the retraction of the steel strand, which leads to the rapid relaxation of the prestress at the initial monitoring stage. After July 2018, the prestress showed a periodic and slow upwards trend. At this time, the rock mass of the slope was affected by external factors such as construction disturbance, temperature change and rainfall, which caused the prestress of the anchor cable to fluctuate greatly [58]. As of September 2020, the prestress loss rate was within 2%, the change in the measured value conformed to the general law of anchor cable stress, and the prestress loss range was within the normal range, indicating that the anchor cable stress was basically normal, and the slope did not significantly deform.

Type 4 measuring points are D03ZPR, D05ZPR, D06ZPR and D07ZPR, all of which are located within the range of the F1 fault and its influence zone. Fig. 13 shows that after the self-tensioning and locking of the anchor cable dynamometer, the prestress of the anchor cable relaxes rapidly and shows a significant downwards trend in the early monitoring period. At this time, prestress occurs due to the retraction of the steel strand lock loss. After September 2018, the prestress showed a long-term slow loss trend. At this time, the anchored rock mass produced creep deformation, which caused the anchor cable to rebound and shrink, which in turn caused the long-term loss of the anchor cable prestress. Around September 2019, the rock mass of the slope was affected by the construction disturbance, and the F1 fault in the slope body produced tension deformation. At this time, the prestress of the anchor cable continued to increase. As of September 2020, the prestress loss rate was within 5%, the change in the measured value was in line with the general law of anchor cable stress, and the prestress loss range was within the normal range, indicating that the anchor cable stress was basically normal, and the slope was not significantly deformed.

D. BPVAR MODEL

1) THE STATIONARITY TEST OF PANEL DATA

If the panel data are not stable, deviations can occur in the model estimation results. Therefore, before establishing the BPVAR model, a unit root test should be performed on the variables to ensure that the data are stable. The LLC test method allows different intercepts and time trends, heteroscedasticity and high-order series correlation and is suitable for the panel unit root test of medium dimensions (time series between 25 and 250, cross-section number between 10 and 250). The IPS test allows the existence of heteroscedasticity when the alternative hypothesis is established, and the test is a Lagrange multiplier test [59]. The ADF-Fisher test is an extended method of the ADF test, and its test effect is better than that of the traditional test method. Therefore, in this paper, the LLC test, IPS test and

TABLE 3. P value of panel data unit root test.

Category of measuring points	LLC test	IPS test	ADF-Fisher test
Type 1 measuring points	0.02	0.00	0.07
Type 2 measuring points	0.00	0.00	0.01
Type 3 measuring points	0.00	0.00	0.00
Type 4 measuring points	0.01	0.01	0.00

TABLE 4. Optimal lag order test for panel data.

Category of measuring points	Lag order	AIC	BIC	HQIC
Type 1 measuring points	1	4.32	4.45*	4.37*
	2	4.31	4.48	4.38
	3	4.30*	4.53	4.39
Type 2 measuring points	1	5.41	5.56	5.47
	2	5.33*	5.55*	5.42*
	3	5.37	5.66	5.49
Type 3 measuring points	1	6.53	6.68*	6.59*
	2	6.51*	6.73	6.60
	3	6.54	6.83	6.65
Type 4 measuring points	1	6.04	6.17*	6.10
	2	6.00*	6.18	6.07*
	3	6.01	6.23	6.09

Note: with * is the optimal lag order.

ADF-Fisher test are used to test the unit root of the panel data of anchor cable prestress [60]. The original hypothesis of the test method is nonstationary panel data [61]. The test results are shown in Table 3. According to Table 3, the P values corresponding to the test statistics are less than 0.1, so the null hypothesis of ''nonstationary panel data'' can be rejected at the significance level of 10%, and the panel data are considered to be stationary.

2) DETERMINING THE OPTIMAL LAG ORDER

The optimal lag order of the model is selected by AIC, BIC and HQIC criteria, and the optimal lag order is determined according to the criterion of obtaining the minimum amount of information. The specific results are shown in Table 4. It can be seen in Table 4 that the optimal lag order of the first and third types of measurement points is the first order, and the second and fourth types of measurement points are the second order.

3) MODEL FITTING AND PREDICTIVE ANALYSIS

In this paper, the BEAR toolbox developed by Dieppe et al. [62] is used to estimate by PVAR technology to further alleviate the small sample problem of slope monitoring data during construction. According to the Bayesian approach, model parameters are treated as random variables characterized by some underlying probability distribution [63]. The method incorporates prior information on model parameters and updates these probability distributions based on observed data. In addition, this paper derives the model posterior distribution through the Gibbs sampling method to obtain the model fitted value, predicted value and confidence interval. In a previous paper, the measurement points of the slope anchor cable dynamometer were divided into four types by the Ward clustering method, and the same type of measurement points had a highly similar prestress variation law. Since

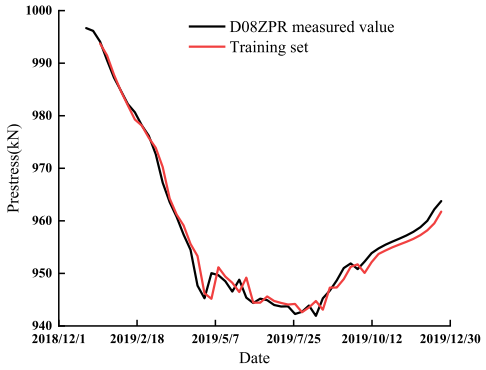

FIGURE 14. D08ZPR measuring point model training results.

the BPVAR model allows the use of temporal and cross-sectional dimensions, both temporal and spatial information are considered for modelling. Therefore, this paper establishes panel data for the same type of measuring points and obtains the fitting and prediction results through the BPVAR model.

According to the cluster analysis results, a BPVAR model is established for each type of measuring point, and the panel data are composed of the prestress monitoring data of all measuring points in the same category. The posterior distribution of the model can be derived by the Gibbs sampling method. The number of preiterations of Gibbs sampling is 2000, and the number of effective iterations is 1000. In this paper, the panel data of the above four types of measuring points are divided into three parts: a training set, test set and verification set. The training set is used to fit the model and adjust the hyperparameters. The test set is used to evaluate the trained model and determine whether to retrain the model or change the hyperparameters in the model according to the model training effect. The validation set is used to evaluate the robustness and prediction error of the model. After multiple debugging of the training set data samples, the overall tightness in the model is determined to be 0.5, the lag attenuation parameter is 1, and the constant term is 0. The coefficient matrix of the model can be obtained by the calculation results of the BPVAR model. The calculation formula of the model fitting value of the first type of measuring point to the fourth type of measuring point is shown in Table 5.

Taking the second type of measuring points as an example, the model training results of D08ZPR and D09ZPR are shown in Fig. 14 ∼ Fig. 15. The data samples of each measuring point in the training set are 51. The multiple correlation coefficients between the fitting value and the measured value of the data samples of the model training set of the second type of measuring points are 0.98 and 0.94, respectively, indicating that the fitting effect of the data samples of the model training set is better.

Taking the second type of measuring point as an example, the model test results of D08ZPR and D09ZPR are shown in Fig. 16 ∼ Fig. 17. There are 20 data samples for each measuring point in the test set. The multiple correlation coefficients between the predicted value and the measured

TABLE 5. The fitting value calculation formula for BPVAR model.

Category of measuring points	Computing formula
Type 1 measuring points	$y_{i,t} = 1.002y_{1,t-1} + 1.003y_{2,t-1} + 1.002y_{3,t-1} + 1.004y_{4,t-1} + \varepsilon_{i,t}$ ($i = 1,2,3,4$)
Type 2 measuring points	$y_{i,t} = 1.356y_{1,t-1} - 0.357y_{1,t-2} + 1.302y_{2,t-1} - 0.303y_{2,t-2} + \varepsilon_{i,t}$ ($i = 1,2$)
Type 3 measuring points	$y_{i,t} = 0.964y_{1,t-1} + 0.96y_{2,t-1} + \varepsilon_{i,t}$ ($i = 1,2$)
Type 4 measuring points	$y_{i,t} = 0.85y_{1,t-1} + 0.149y_{1,t-2} + 0.85y_{2,t-1} + 0.15y_{2,t-2} + 0.85y_{3,t-1} + 0.15y_{3,t-2} + 0.851y_{4,t-1} + 0.15y_{4,t-2} + \varepsilon_{i,t}$ ($i = 1,2,3,4$)

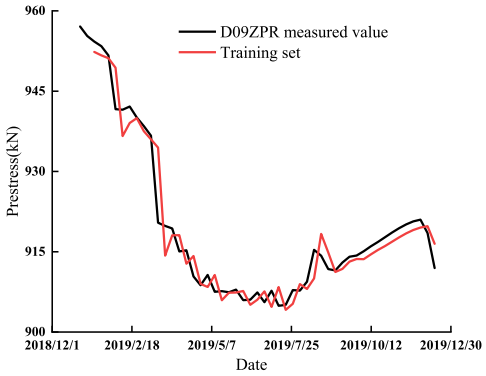

FIGURE 15. D09ZPR measuring point model training results.

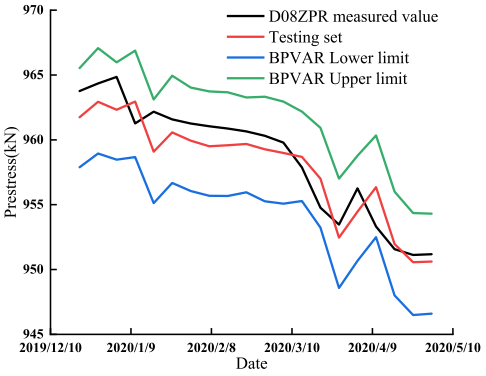

FIGURE 16. D08ZPR measuring point model test results.

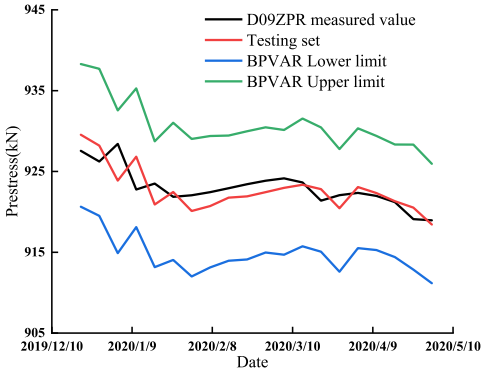

FIGURE 17. D09ZPR measuring point model test results.

value in the data sample of the model test set are 0.84 and 0.88, respectively, indicating that the test effect of the BPVAR model is better.

Taking the second type of measuring point as an example, the model verification results of D08ZPR and D09ZPR are shown in Fig. 18 ∼ Fig. 19. The data in the validation set

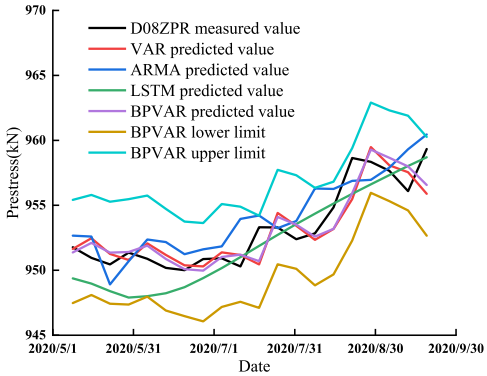

FIGURE 18. D08ZPR measuring point model verification results.

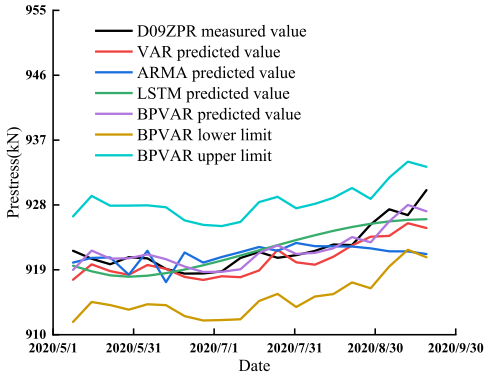

FIGURE 19. D09ZPR measuring point model verification results.

are used for BPVAR model prediction, and the data samples of each measuring point are also 20. To compare with the one-step prediction results of the BPVAR model, the traditional vector autoregressive (VAR) model, autoregressive moving average (ARMA) model and long short-term memory (LSTM) model are used to predict and analyse the prestress of D08ZPR and D09ZPR, as shown in Fig. 18 ∼ Fig. 19 (the prediction interval of the BPVAR model in Fig. 18 ∼ Fig. 19 is the 95% confidence interval). According to the prediction results of the BPVAR model, the one-step prediction value of the BPVAR model is basically consistent with the measured value, and the measured value of the prestress is within the 95% confidence interval, indicating that the BPVAR model can fully consider the uncertainty factors of the prestress monitoring during the construction period of the slope and has good interval prediction ability.

4) EVALUATION OF PREDICTION ACCURACY

To comprehensively analyse the prediction accuracy of the BPVAR model, the mean absolute error (MAE), mean absolute percentage error (MAPE) and root mean square error

TABLE 6. Model prediction accuracy evaluation.

Model	Measuring point D08ZPR			Measuring point D09ZPR		
	MAE (kN)	MAPE (%)	RMSE (kN)	MAE (kN)	MAPE (%)	RMSE (kN)
VAR	1.21	0.13	1.52	1.70	0.18	2.17
ARMA	1.49	0.16	1.76	2.14	0.23	3.03
LSTM	1.57	0.16	1.79	1.59	0.17	1.86
BPVAR	1.10	0.11	1.37	1.09	0.12	1.39

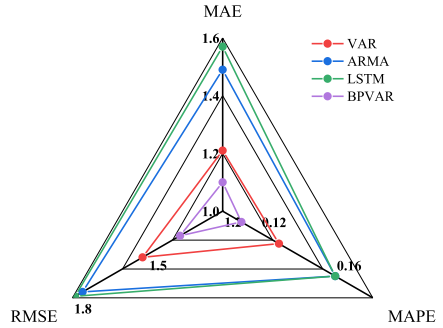

FIGURE 20. Radar chart of the prediction error of the D08ZPR measuring point.

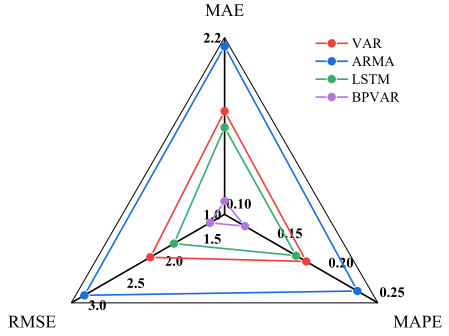

FIGURE 21. Radar chart of the prediction error of the D09ZPR measuring point.

(RMSE) of the VAR model, ARMA model, LSTM model and BPVAR model are calculated. Based on the above three error indicators, a reasonable evaluation is made. Taking the second type of measuring points as an example, the prediction error indices of the above models are shown in Table 6. In Fig. 18 ∼ Fig. 19 and Table 6, it can be seen that the defect of the VAR model is that the model parameters are too numerous and the prediction effect is not good [30]; although the ARMA model can predict the trend of prestress, the prediction accuracy decreases with the increase in the number of predictions [31]. For the small sample data of slope anchor cable prestress during construction, the prediction accuracy of the LSTM model is often low [32]. Compared with the single time series prediction results of the traditional VAR model, ARMA model and LSTM model, the BPVAR model integrates the spatial and temporal information of multiple measuring points, and its prediction accuracy is improved to varying degrees. A radar chart is drawn according to the error index of each model in Table 6. From the radar chart of the error index of the model, it can be seen that the MAE, MAPE and RMSE of the BPVAR model are smaller than those of the VAR model, the ARMA model and the LSTM model, indicating that the prediction accuracy of the BPVAR model is high. It can provide a reference value for the prediction and analysis of anchor cable prestress during slope construction.

VI. CONCLUSION

In this paper, the spatial clustering algorithm is used to cluster the prestressed measuring points of a slope, and the prestressed measuring points of the slope are divided according to the clustering results. Then, a safety monitoring method for slope anchor cable prestress based on the BPVAR model is established. Finally, this is verified by an engineering example. The main conclusions can be drawn as follows:

(1) Compared with the classic K-means clustering method, the Ward clustering method has a better spatial clustering effect. The Ward clustering results are more consistent with the variation rule of prestress monitoring values. The engineering application research shows that the prestressed measuring points of the left bank slope of a water conservancy project are divided into four categories, and each type of measuring point has a highly similar change law of prestress.

(2) Due to the influence of the retraction of the steel strand of the anchor cable dynamometer and the compression of the stratum, the prestress is rapidly relaxed in the early stage of monitoring. Under the influence of excavation disturbance, the prestress of some measuring points continues to increase, and its variation law is consistent with that of the nearby multi-point displacement meter. The prestress increases or decreases with the tensile or compressive deformation of the structural plane. It can be seen from the change law of slope prestress that the prestress loss range of most measuring points is within the normal range, and the slope does not show obvious deformation, which is in line with the general change law of slope prestress.

(3) According to the training, testing and verification results of the BPVAR model, the multiple correlation coefficients between the modelling results of the training set and the test set data and the measured values are all above 0.80, indicating that the modelling effect of the BPVAR model is better. The mean absolute error, mean absolute percentage error and root mean square error of the BPVAR model are smaller than those of the traditional VAR model, ARMA model and LSTM model. At the same time, the measured values of slope prestress are all within the 95% confidence interval, which indicates that the interval prediction effect of the BPVAR model is good and can provide a reference for slope engineering.

In this research, the BPVAR model demonstrates better interval prediction ability, but the hyperparameter value in the model still has certain subjectivity, and its value standard is to obtain the optimal prediction effect. This will be the focus of future research to determine the most accurate model hyperparameters in a better way.

REFERENCES

[1] J. Yang, C. Ma, L. Cheng, G. Lu, and B. Li, "Research advances in the deformation of high-steep slopes and its influence on dam safety," *Rock Soil Mech.*, vol. 40, no. 6, pp. 2341–2353, Jun. 2019.

[2] B. Hu, G. Su, J. Jiang, J. Sheng, and J. Li, "Uncertain prediction for slope displacement time-series using Gaussian process machine learning," *IEEE Access*, vol. 7, pp. 27535–27546, 2019, doi: 10.1109/ACCESS.2019.2894807.

[3] C. Zhu, M. He, Z. Tao, Q. Meng, and X. Zhang, "Recognition and prevention of rockfall vulnerable area in open-pit mines based on slope stability analysis," *Geomech. Eng.*, vol. 26, no. 5, pp. 451–452, Sep. 2021, doi: 10.12989/gae.2021.26.5.441.

[4] K. Dong, D. Yang, J. Chen, J. Zhou, J. Li, X. Lu, L. Pei, and Q. Kou, "Monitoring-data mechanism-driven dynamic evaluation method for slope safety," *Comput. Geotech.*, vol. 148, Aug. 2022, Art. no. 104850, doi: 10.1016/j.compgeo.2022.104850.

[5] C. Zhu, M. He, X. Zhang, Z. Tao, Q. Yin, and L. Li, "Nonlinear mechanical model of constant resistance and large deformation bolt and influence parameters analysis of constant resistance behavior," *Rock Soil Mech.*, vol. 42, no. 7, pp. 1911–1924, Jul. 2021, doi: 10.16285/j.rsm.2020.1764.

[6] G. Shi, G. Gu, H. Zhou, Z. Tao, H. Pan, T. Tang, and Q. Yin, "Stability monitoring and analysis of high and steep slope of a hydropower station," *Geofluids*, vol. 2020, pp. 1–16, Sep. 2020, doi: 10.1155/2020/8840269.

[7] W. Yang, X. Wang, N. Liu, and Q. Wang, "An analytical solution for the time-dependent anchoring force in prestressed cables due to rock creep," *Mech. Time-Dependent Mater.*, vol. 27, no. 2, pp. 367–399, Nov. 2022, doi: 10.1007/s11043-022-09577-6.

[8] Z. Chen, Z. Wang, H. Xi, Z. Yang, L. Zou, Z. Zhou, and C. Zhou, "Recent advances in high slope reinforcement in China: Case studies," *J. Rock Mech. Geotech. Eng.*, vol. 8, no. 6, pp. 775–788, Dec. 2016, doi: 10.1016/j.jrmge.2016.11.001.

[9] M. Song, X. Xiang, G. Zhang, X. Yang, and L. Wen, "Study on the mechanical characteristics and prestress loss of slope-anchored structure," *Chin. J. Rock Mech. Eng.*, vol. 41, no. S1, pp. 2791–2800, May 2022, doi: 10.13722/j.cnki.jrme.2021.0649.

[10] G. Chen, T. Chen, Y. Chen, R. Huang, and M. Liu, "A new method of predicting the prestress variations in anchored cables with excavation unloading destruction," *Eng. Geol.*, vol. 241, pp. 109–120, Jul. 2018, doi: 10.1016/j.enggeo.2018.05.015.

[11] G. Jurell, "Investigation into the failure of a prestressed rock anchor," *Int. Water Power Dam Construct.*, vol. 37, no. 2, pp. 45–47, Feb. 1985.

[12] F. Zhang, W. Zhao, N. Liu, and Z. Chen, "Long-term performance and load prediction model of prestressed cables," *Chin. J. Rock Mech. Eng.*, vol. 2004, no. 1, pp. 39–43, Jan. 2004.

[13] H. Sun, L. N. Y. Wong, Y. Shang, Q. Lu, and W. Zhan, "Systematic monitoring of the performance of anchor systems in fractured rock masses," *Int. J. Rock Mech. Mining Sci.*, vol. 47, no. 6, pp. 1038–1045, Sep. 2010, doi: 10.1016/j.ijrmms.2010.05.012.

[14] X. Li, L. Zhang, and S. Zhang, "Efficient Bayesian networks for slope safety evaluation with large quantity monitoring information," *Geosci. Frontiers*, vol. 9, no. 6, pp. 1679–1687, Nov. 2018, doi: 10.1016/j.gsf.2017.09.009.

[15] R. C. Jung, M. Kukuk, and R. Liesenfeld, "Time series of count data: Modeling, estimation and diagnostics," *Comput. Statist. Data Anal.*, vol. 51, no. 4, pp. 2350–2364, Dec. 2006, doi: 10.1016/j.csda.2006.08.001.

[16] H. Wu, "Time series analysis and synthesis," Wuhan Univ. Press, Wuhan, China, Tech. Rep., 2004.

[17] Q. Xie, Y. Xia, and K. Cheng, "Time series analysis of defomation monitoringon rock mass and development of dynamic model," *J. Eng. Geol.*, vol. 2001, no. 3, pp. 308–311, Dec. 1999.

[18] A. Aggarwal, M. Alshehri, M. Kumar, O. Alfarraj, P. Sharma, and K. R. Pardasani, "Landslide data analysis using various time-series forecasting models," *Comput. Electr. Eng.*, vol. 88, Dec. 2020, Art. no. 106858, doi: 10.1016/j.compeleceng.2020.106858.

[19] M. Meng, Z. Chen, D. Huang, B. Zeng, and C. Chen, "Displacement prediction of landslide in three Gorges reservoir area based on H-P filter, ARIMA and VAR models," *Rock Soil Mech.*, vol. 37, no. S2, pp. 552–560, Oct. 2016, doi: 10.16285/j.rsm.2016.S2.070.

[20] X. Lu, F. Miao, X. Xie, D. Li, and Y. Xie, "A new method for displacement prediction of 'step-like' landslides based on VMD-FOA-SVR model," *Environ. Earth Sci.*, vol. 80, no. 17, p. 542, Sep. 2021, doi: 10.1007/s12665-021-09825-x.

[21] Q. Xu, M. Tang, K. Xu, and X. Huang, "Research on space-time evolution laws and early warning-prediction of landslides," *Chin. J. Rock Mech. Eng.*, vol. 27, no. 6, pp. 1104–1112, 2008.

[22] X. Zhao, G. Li, Z.-F. Zhao, C.-X. Li, Q. Chen, and X. Ye, "Identifying the spatiotemporal characteristics of individual red bed landslides: A case study in Western Yunnan, China," *J. Mountain Sci.*, vol. 19, no. 6, pp. 1748–1766, Jun. 2022, doi: 10.1007/s11629-022-7339-0.

[23] W. Feng, H. Bai, B. Lan, Y. Wu, Z. Wu, L. Yan, and X. Ma, "Spatial–temporal distribution and failure mechanism of group-occurring landslides in Mibei village, Longchuan county, Guangdong, China," *Landslides*, vol. 19, no. 8, pp. 1957–1970, May 2022, doi: 10.1007/s10346-022-01904-9.

[24] H. Cheng, G. Zhang, Y. Liu, Q. Zhou, Z. Lei, and D. Chai, "Analysis and numerical simulation of toppling deformation and failure characteristics of anti-dipping rock slope under impoundment," in *Proc. 11th Conf. Asian Rock Mech. Soc.*, Beijing, China, Oct. 2021, pp. 1–12, doi: 10.1088/1755-1315/861/7/072097.

[25] Q. Ge, D. Wang, H. Sun, F. Shuai, and Z. Chen, "Displacement prediction of filling road bed slope surface based on dynamic spatial panels model," *J. Eng. Geol.*, vol. 27, no. 2, pp. 367–375, Apr. 2019.

[26] C. Liu, "Research review on vector autoregressive model for panel data," *Statist. Decis.*, vol. 37, no. 2, pp. 25–29, 2021, doi: 10.13546/j.cnki.tjyjc.2021.02.005.

[27] F. Canova and M. Ciccarelli, "Panel vector autoregressive models: A survey," *Adv. Econometrics*, vol. 32, pp. 1–12, Dec. 2013, doi: 10.1108/S0731-9053(2013)0000031006.

[28] S. Y. Lee, Z. A. Karim, N. Khalid, and M. A. S. Zaidi, "The spillover effects of Chinese shocks on the belt and road initiative economies: New evidence using panel vector autoregression," *Mathematics*, vol. 10, no. 14, p. 2414, Jul. 2022, doi: 10.3390/math10142414.

[29] F. F. E. Silva, T. Sáfadi, J. A. Muniz, G. J. M. Rosa, L. H. D. Aquino, G. B. Mourão, and C. H. O. Silva, "Bayesian analysis of autoregressive panel data model: Application in genetic evaluation of beef cattle," *Scientia Agricola*, vol. 68, no. 2, pp. 237–245, Apr. 2011, doi: 10.1590/S0103-90162011000200015.

[30] W. Yang and L. Cheng, "Forecasting China's inter-bank bond yields with Bayesian vector autoregressions," *Stat. Res.*, vol. 32, no. 8, pp. 69–76, Aug. 2015, doi: 10.19343/j.cnki.11-1302/c.2015.08.009.

[31] L. Yu, "Evaluation and analysis of electric power in China based on the ARMA model," *Math. Problems Eng.*, vol. 2022, pp. 1–6, Sep. 2022, doi: 10.1155/2022/5017751.

[32] J. Cao, F. Liu, and Z. Shen, "A LSTM-based model for TBM performance prediction and the effect of rock mass grade on prediction accuracy," *China Civil Eng. J.*, vol. 55, no. S2, pp. 92–102, Nov. 2022.

[33] B. Hu and H. Tan, "Slope deformation analysis and forecast based on ARIMA model," *Bull. Surveying Mapping*, vol. 507, no. 6, pp. 112–116, 2019, doi: 10.13474/j.cnki.11-2246.2019.0197.

[34] M. H. Pesaran, "Estimation and inference in large heterogeneous panels with a multifactor error structure," *Econometrica*, vol. 74, no. 4, pp. 967–1012, Jul. 2006.

[35] A. Zellner, "The Bayesian method of moments (Bmom)," *Adv. Econometrics*, vol. 12, pp. 85–105, Jul. 1997, doi: 10.1108/S0731-9053(1997)0000012005.

[36] F. Canova and M. Ciccarelli, "Forecasting and turning point predictions in a Bayesian panel VAR model," *J. Econometrics*, vol. 120, no. 2, pp. 327–359, Jun. 2004, doi: 10.1016/S0304-4076(03)00216-1.

[37] G. Koop and D. Korobilis, "Model uncertainty in panel vector autoregressive models," *Eur. Econ. Rev.*, vol. 81, pp. 115–131, Jan. 2016, doi: 10.1016/j.euroecorev.2015.09.006.

[38] J. Hu and F. Ma, "Zoned safety monitoring model for uplift pressures of concrete dams," *Trans. Inst. Meas. Control*, vol. 41, no. 14, pp. 3952–3969, May 2019, doi: 10.1177/0142331219842281.

[39] R. K. Gautam, N. Singh, N. K. Choudhary, and A. Narain, "Model order reduction using factor division algorithm and fuzzy c-means clustering technique," *Trans. Inst. Meas. Control*, vol. 41, no. 2, pp. 468–475, Apr. 2018, doi: 10.1177/0142331218762605.

[40] J. Chen, "The application research of ward system clustering method in the analysis of rural residents' income," *J. Dali Univ.*, vol. 14, no. 6, pp. 28–32, Jun. 2015.

[41] T. Hu, "Spatial and temporal clustering model of concrete arch dam deformation data based on panel data analysis method," *J. Yangtze River Sci. Res. Inst.*, vol. 38, no. 2, pp. 39–45, Feb. 2021, doi: 10.11988/ckyyb.20191217.

[42] Q. Chen, *Advanced Econometrics and Stata Applications*, 2nd ed. Beijing, China: Higher Educ. Press, 2014, pp. 422–431.

[43] A. Levin, C. Lin, and C. Chu, "Unit root tests in panel data: Asymptotic and finite-sample properties," *J. Econometrics*, vol. 108, no. 1, pp. 1–24, May 2002, doi: 10.1016/S0304-4076(01)00098-7.
[44] K. Im, M. Pesaran, and Y. Shin, "Testing for unit roots in heterogeneous panels," *J. Econometrics*, vol. 115, no. 1, pp. 53–74, Jul. 2003, doi: 10.1016/S0304-4076(03)00092-7.
[45] G. S. Maddala and S. Wu, "A comparative study of unit root tests with panel data and a new simple test," *Oxford Bull. Econ. Statist.*, vol. 61, no. S1, pp. 631–652, Dec. 2002, doi: 10.1111/1468-0084.0610s1631.
[46] I. Choi, "Unit root tests for panel data," *J. Int. Money Finance*, vol. 20, no. 2, pp. 249–272, Apr. 2001, doi: 10.1016/S0261-5606(00)00048-6.
[47] H. Akaike, "A new look at the statistical model identification," *IEEE Trans. Autom. Control*, vol. AC-19, no. 6, pp. 716–723, Dec. 1974.
[48] G. Schwarz, "Estimating the dimension of a model," *Ann. Statist.*, vol. 6, no. 2, pp. 461–464, Mar. 1978.
[49] E. J. Hannan and B. G. Quinn, "The determination of the order of an autoregression," *J. Roy. Stat. Soc., B, Methodol.*, vol. 41, no. 2, pp. 190–195, Jan. 1979, doi: 10.1111/j.2517-6161.1979.tb01072.x.
[50] M. Jarociński, "Responses to monetary policy shocks in the east and the west of Europe: A comparison," *J. Appl. Econometrics*, vol. 25, no. 5, pp. 833–868, Aug. 2010, doi: 10.1002/jae.1082.
[51] A. Zellner and C. Hong, "Forecasting international growth rates using Bayesian shrinkage and other procedures," *J. Econometrics*, vol. 40, no. 1, pp. 183–202, Jan. 1989, doi: 10.1016/0304-4076(89)90036-5.
[52] Z. Hu and M. Qu, "Analysis on safety monitoring data of access road slope to Yangfanggou hydropower station," *Yangtze River*, vol. 47, no. 20, pp. 78–81, Aug. 2016, doi: 10.16232/j.cnki.1001-4179.2016.20.023.
[53] T. Wang, T. Wang, and G. Lei, "Application of improved fuzzy C means clustering method in the cluster analysis of water saving irrigation level," *Water Resour. Hydropower Northeast China*, vol. 35, no. 7, pp. 55–58, Sep. 2016, doi: 10.14124/j.cnki.dbslsd22-1097.2017.07.023.
[54] S. Wang, C. Liu, and S. Xing, "Review on K-means clustering algorithm," *J. East China Jiaotong Univ.*, vol. 39, no. 5, pp. 119–126, Oct. 2022, doi: 10.16749/j.cnki.jecjtu.20220914.001.
[55] Y. Tong, W. Yang, and Z. Wu, "Discussion of appliance of anchor dynamometer in the extension engineering of Zhalin hydropower station," *Jiangxi Hydraulic Sci. Technol.*, vol. 27, no. 2, pp. 105–107, Jun. 2001.
[56] Z. Feng, G. Jiang, R. Zhao, H. Long, Z. Wang, and Z. Zhang, "Study on pre-stress long term loss of anchor cable considering coupled multiple factors," *Rock Soil Mech.*, vol. 42, no. 8, pp. 2215–2224, Aug. 2021.
[57] K. Shi, X. Wu, and Z. Wang, "Analysis of prestress loss model and prestress compensation time of anchor cable," *J. Central South Univ., Sci. Technol.*, vol. 53, no. 6, pp. 2134–2142, Jul. 2021.
[58] F. Jing, J. Zhu, Z. Bian, and H. Chen, "Analysis on the prestressing variety characteristics of prestressed cable in soft rock slope," *Chin. J. Underground Space Eng.*, vol. 4, no. 5, pp. 820–824, Oct. 2008.
[59] Z. Wang, "Unit root test and growth convergence of panel data," *Statist. Decis.*, vol. 2006, no. 12, pp. 19–22, Jun. 2006, doi: 10.13546/j.cnki.tjyjc.2006.12.007.
[60] Y. Yang, "Forecast of urban railway passenger volume based on PVAR-XGBoost combined model," M.S. thesis, Beijing Jiaotong Univ., Beijing, China, Tech. Rep., 2021.
[61] T. Chen, "Study on the relationship between population mobility and housing price based on PVAR model," M.S. thesis, Anhui Jianzhu Univ., Anhui, China, Tech. Rep., 2022.
[62] A. Dieppe, R. Legrand, and B. Roye, "The BEAR toolbox," European Central Bank, Frankfurt, Germany, Tech. Rep., Aug. 2016, doi: 10.2866/292952.
[63] A. Adarov, "Dynamic interactions between financial cycles, business cycles and macroeconomic imbalances: A panel VAR analysis," *Int. Rev. Econ. Finance*, vol. 74, pp. 434–451, Jul. 2021, doi: 10.1016/j.iref.2021.03.021.

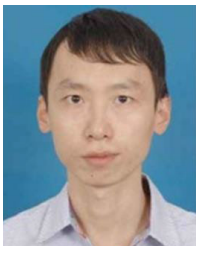

LIN CHENG received the Ph.D. degree from the College of Water Conservancy and Hydropower Engineering, Hohai University, Nanjing, China, in 2014. He is currently with the Xi'an University of Technology. He was involved in some research projects about the application of optical fiber in hydraulic engineering. His current research interests include structural health monitoring, structure vibration, fiber optical sensors, and finite element method.

YUE JIANG is currently pursuing the Graduate degree in hydraulic structure engineering with the Xi'an University of Technology. His current research interest includes slope safety monitoring.

CHUNHUI MA is currently a Postdoctoral Teacher with the Xi'an University of Technology. His current research interests include numerical simulation and safety monitoring of hydraulic structures.

JIE YANG is currently a Doctoral Supervisor with the Xi'an University of Technology. His current research interests include hydraulic structure, reservoir dam safety, and reinforcement theory.

JIAMIN CHEN is currently pursuing the Graduate degree in hydraulic structure engineering with the Xi'an University of Technology. His current research interest includes dam safety monitoring.

SHUAI YUAN is currently pursuing the Graduate degree in hydraulic structure engineering with the Xi'an University of Technology. His current research interest includes dam safety monitoring.

ZENGGUANG XU is currently a Doctoral Supervisor with the Xi'an University of Technology. His current research interests include the seepage effect and control of reservoir dam systems of water conservancy projects.